Adaptive fuzzy clustering in constructing parametric images for low SNR functional imaging

Lingfeng Wen [#*^1], Stefan Eberl [#*2], Michael Fulham [#*+3], Dagan Feng [#^4], Jing Bai [~5]

[#] *Biomedical and Multimedia Information Technology (BMIT) Research Group, School of Information Technologies, University of Sydney, Australia*

[1] wenlf@ieee.org

[*] *Department of PET and Nuclear Medicine, Royal Prince Alfred Hospital, Sydney, Australia*

[2] eberl@staff.usyd.edu.au

[+] *Faculty of Medicine, University of Sydney, Australia*

[3] mfulham@med.usyd.edu.au

[^] *Department of Electronic and Information Engineering, Hong Kong Polytechnic University, Hong Kong*

[4] feng@it.usyd.edu.au

[~] *Department of Biomedical Engineering, Tsinghua University, China*

[5] deabj@tsinghua.edu.cn

***Abstract*—Functional imaging can provide quantitative functional parameters to aid early diagnosis. Low signal to noise ratio (SNR) in functional imaging, especially for single photon emission computed tomography, poses a challenge in generating voxel-wise parametric images due to unreliable or physiologically meaningless parameter estimates. Our aim was to systematically investigate the performance of our recently proposed adaptive fuzzy clustering (AFC) technique, which applies standard fuzzy clustering to sub-divided data. Monte Carlo simulations were performed to generate noisy dynamic SPECT data with quantitative analysis for the fitting using the general linear least square method (GLLS) and enhanced model-aided GLLS methods. The results show that AFC substantially improves computational efficiency and obtains improved reliability as standard fuzzy clustering in estimating parametric images but is prone to slight underestimation. Normalization of tissue time activity curves may lead to severe overestimation for small structures when AFC is applied.**

I. INTRODUCTION

Functional imaging techniques like positron emission tomography (PET), single photon emission computed tomography (SPECT), and functional magnetic resonance imaging (fMRI) provide valuable diagnostic information at the organ/tissue levels. One advantage of functional imaging is its ability to provide quantitative parameters, reflecting in-vivo biochemical/physiological processes, which can facilitate early diagnosis by detecting subtle changes [1]. This process usually requires parameter estimation techniques to analyze a sequence of image-based signals according to an underlying kinetic model and a given input functions (IF) for the model. For emission-tomography based PET and SPECT, the tissue time activity curve (TTAC) is regarded as the measured signal and the plasma time activity curve (PTAC) is the IF. Low signal to noise ratio (SNR) in voxel-wise TTAC, especially for SPECT, gives rise to unreliable and physiologically meaningless parameter estimates due to intrinsic statistical noise, which poses a major challenge for constructing parametric images.

Various techniques to improve the SNR of noisy imaging data have been investigated. Low-pass filtering is a relatively simple approach but at the expense of image resolution. Post-reconstruction filtering was found to increase estimated bias without significantly improving estimated reliability [2]. The optimal imaging sampling schedule (OISS) method is an alternatively approach to improve SNR in temporal domain by combing short-duration scans into long-duration frames without degrading estimated accuracy [3]. The need to customize OISS for a particular tracer hinders its general use in functional imaging. In contrast, clustering can achieve improved SNR in the spatial domain.

The various clustering analysis algorithms, such as hierarchical, squared error-based and fuzzy clustering, have been used to tackle diverse problems such as exploratory pattern-analysis, decision-making and machine-learning through classifying patterns or feature vectors into a group of clusters in terms of similarity measures [4, 5]. In medical imaging, clustering has been used to segment MR and PET images [6-8], and to generate parametric images [9-12], where parameter estimation is integrated with cluster analysis and estimates associated with the cluster centroid curve proportionally represent all voxels belonging to the cluster. The "hard" clustering techniques, such as K-mean [11] and hierarchical clustering [12], assign instances to one specific cluster during iterative analysis. This may lead to misclassification with biased centroid curves. In contrast, fuzzy clustering has the benefit of each instance contributing to all cluster centroids in terms of fuzzy membership; in our recent work we validated this approach for constructing reliable parametric images using a standard fuzzy clustering technique [13]. However, because each voxel and cluster in the analysis need iterative updating there is a large computational burden which is impractical for routine clinical use.

978-1-4244-2295-1/08/$25.00 © 2008 IEEE

Recently, we proposed a novel adaptive fuzzy clustering (AFC) method to address this problem [14]. In this study, our aim was to systematically investigate the performance of the AFC using two parameter estimation methods, the generalized linear least square method (GLLS) [15] and enhanced model-aided GLLS (MGLLS) [16] with SPECT data. We also investigated the ability of TTAC normalization to further improve reliability of the parametric images. Computer Monte Carlo simulation were performed to generate dynamic SPECT data of human brain with the kinetics of the nicotinic receptor tracer 5-[^{123}I]-iodo-A-85380 [17]. The performance of AFC was evaluated by comparing it to standard fuzzy clustering in terms of estimated accuracy and reliability, and computational cost.

II. Methods

A. Computer Simulation

A dedicated mathematical phantom of the human brain was used in the simulation [18]. Static projection data for seventeen individual brain structures were generated by high-count Monte Carlo simulation based on the characteristics of a Triad XLT triple head gamma camera (Trionix Research Laboratories, Twinburg, OH, USA). The experimentally observed kinetics of the nicotinic receptor tracer 5-[^{123}I]-iodo-A-85380 were used to generate dynamic projection data including effects of attenuation, scatter, limited spatial and energy resolution. The high-energy photon penetration of ^{123}I in collimator was also included [12]. A thirty-six frame sampling schedule was used, consisting of 15 one-minute scans, 9 five-minute scans and 12 ten-minute scans.

Five different levels of Poisson noise were added to the projection data based on experimentally observed noise levels. For each noise level, twenty sets of noisy dynamic projection data were simulated and reconstructed by the OS-EM iterative method [19]. Attenuation and scatter correction and correction of septal penetration of the high-energy photons of ^{123}I were included in the reconstruction. No partial volume effect correction was applied.

B. Fuzzy Clustering

Euclidean distance is a commonly used similarity measure in clustering. A weighted Euclidean distance D_{jk} was used as a measure of similarity between the jth candidate voxel and the centroid of the ith cluster as shown in (1).

$$D(C_j, R_k) = \sum_{i=1}^{n} w_i [C_j(t_i) - R_k(t_i)]^2 \qquad (1)$$

where n is the number of scan frames, t_i is the mid time of each scan, $C_j(t)$ is the TTAC of the jth voxel, $R_k(t)$ is the centroid curve of the kth cluster, w_i is the corresponding weight, being proportional to the frame duration.

Standard fuzzy C-mean (FCM) clustering was used in the investigation by minimizing the cost function J_{FCM} in equation (2) with number of clusters M, Ω_0 is the set of the voxels,

$$J_{FCM} = \arg\min \sum_{j\in\Omega_0} \sum_{k=1}^{M} (u_{jk})^q D(C_j, R_k) \qquad (2)$$

where μ_{jk} is the fuzzy membership value at the jth voxel location for the kth cluster, q is a weighting exponent on each fuzzy membership. In this study, q was chosen to be 1.1 according to our previous investigation. M was set to 256, satisfying the requirement of sufficient number of cluster.

C. Adaptive Fuzzy Clustering

Fig.1 depicts the procedure of AFC, which was proposed to convert standard FCM with number of clusters M into adaptive FCM using n levels with less number of clusters according to (3).

$$\prod_i S_i = M \qquad (3)$$

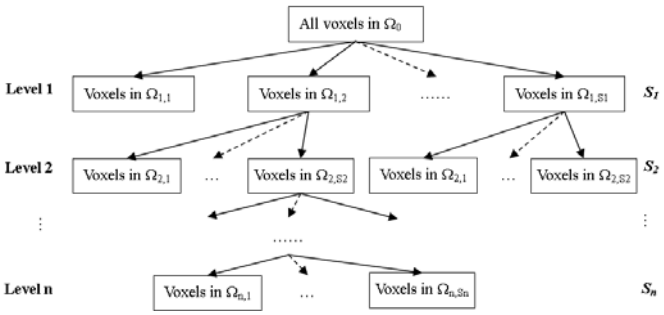

Fig. 1. The workflow of the adaptive fuzzy clustering using n levels

During clustering analysis, original FCM is iteratively achieved with the reduced cluster number of S_{i+1} according to equations (4) and (5) at the level of i+1 in terms of the mth cluster obtained at the previous level of i.

$$u_{jk} = \frac{1}{\sum_{s=1}^{S_{i+1}} \left[\frac{D(C_j, R_k)}{D(C_j, R_s)} \right]^{\frac{1}{q-1}}}, \forall j \in \Omega_{i,m} \qquad (4)$$

$$R_k = \frac{\sum_{j\in\Omega_{i,m}} (u_{jk})^q \cdot C_j(t)}{\sum_{j\in\Omega_{i,m}} u_{jk}^q}, \forall k \in \Phi_{i+1} \qquad (5)$$

Here Φ_{i+1} denotes the set of the clusters at this level of AFC, $\Omega_{i,\,m}$ is the set of the voxels whose maximum fuzzy memberships are associated with the mth cluster at the ith level of AFC.

The AFC initially clusters all the voxels Ω_0 with the cluster number of S_1 at the 1st level. When the last level of AFC was reached, the fuzzy memberships are combined across the levels with $\sum_{k=1}^{M} u_{jk} = 1$ for each voxel. The centroid curves will be updated correspondingly.

In this study, four levels were chosen for AFC with 4 clusters at each level, i.e., S = [4, 4, 4, 4] which is equivalent to 256 clusters.

D. Parametric Images and Quantitative Evaluation

The GLLS and our recently proposed MGLLS methods were used to fit the centroid curves of the clusters obtained by the FCM and AFC according to a three-compartment and four-parameter neuroreceptor model shown in Fig.2.

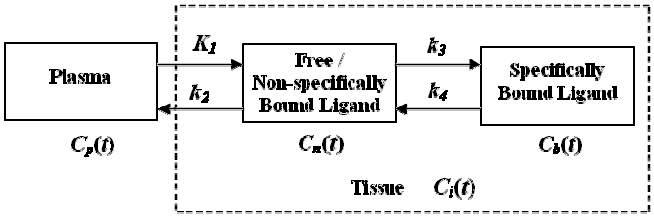

Fig.2. Three-compartment and four-parameter kinetic model for neuroreceptor studies. $C_p(t)$ is PTAC, $C_t(t)$ is TTAC. K_1, k_2, k_3 and k_4 are the rate constants connecting adjacent compartments.

For physiologically meaningless fit, the fuzzy memberships associated with a particular cluster were simply set to zero if any of the rate constants were negative or higher than 1 for a fit to the cluster centroid curve. The rate constants for the cluster with the maximum fuzzy membership were used as the values of the voxel in constructing parametric image.

Two functional parameters, influx rate K_1 and volume of distribution V_d ($V_d=K_1(k_3+k_4)/(k_2k_4)$) were used as the parameters of interest in the quantitative evaluation. Volumes of interests (VOI), derived from the brain phantom, were used to generate the average parameters for the thalamus, cerebellum, and frontal cortex for each realization of noisy dynamic SPECT data. The percentage bias and coefficient of variation (CV) of K_1 and V_d were derived according to equations (6) and (7).

$$Bias = \frac{1}{MC}\left[\sum_{i=1}^{MC}\sum_{j=1}^{N}\frac{p_{i,j}-p_o}{N}\right]/p_o \times 100\% \quad (6)$$

$$CV = \frac{1}{p_0}\sqrt{\frac{\sum_{i=1}^{MC}(\sum_{j=1}^{N}\frac{p_{i,j}}{N})^2 - MC(\sum_{i=1}^{MC}\sum_{j=1}^{MC}\frac{p_{i,j}}{N})^2}{MC-1}} \times 100\% \quad (7)$$

where MC is the total number of data sets at each noise level, N is the number of voxels within a VOI, $p_{i,j}$ is the estimated parameter for the jth voxel in the corresponding VOI for the ith simulation data set, p_0 is the referenced parameter value related to the experimental kinetic curves used in the simulation.

We also investigated the effect of incorporating the normalization of TTAC which assumed that K_1 was a scale factor of the TTAC [10]. Voxel-wise TTAC was normalized by the integral of its amplitude prior to clustering. The estimate of K_1 for one voxel was then derived by multiplying the integral of its TTAC with the estimate of corresponding cluster centroid curve with maximum fuzzy membership.

III. Results

A. Percentage Bias and CV

Fig.3 shows curves of percentage bias and CV for K_1 and V_d over the clustering methods as a function of increasing noise level for the frontal cortex.

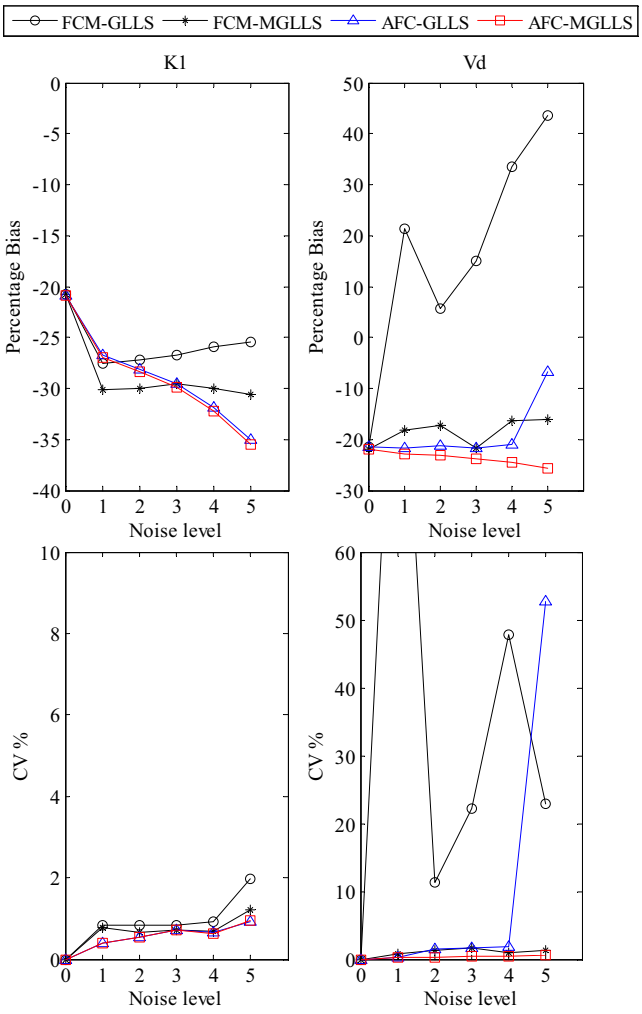

Fig.3. Plots of percentage bias and CV for the frontal cortex as a function of increasing noise level without the normalization of TTAC (the number values of the abscissa denote simulated level of noise with 0 representing noise free data). FCM-GLLS: GLLS fitting with 256-cluster FCM, FCM-MGLLS: MGLLS fitting with 256-cluster FCM, AFC-GLLS: GLLS fitting with the levels S = [4,4,4,4], AFC-MGLLS: MGLLS fitting with the levels S = [4,4,4,4].

Bias of K_1 was similar for the data at the lower noise levels. AFC was observed to increasingly underestimate K_1 both for AFC-GLLS and AFC-MGLLS with increasing noise level, while K_1 achieved by FCM-GLLS and FCM-MGLLS seemed to be less sensitive to noise variation. Low CVs were observed for K_1 by all the methods (<2%). Bias of V_d by FCM-GLLS showed large variation with noise levels. The other three methods achieved very similar bias of V_d with lower CV (<2%) except for AFC-GLLS at the highest noise level (CV=52.7%). This is mainly attributed to the data analysis using AFC not being able to eliminate physiologically meaningless fits using GLLS, which resulted in low reliability of V_d for the data at the 5th noise level.

Similar results were observed for the cerebellum, while different biases of K_1 and V_d were observed for the thalamus in Fig.4. The four methods achieved similar trends of K_1 as a function of noise level. In contrast, only AFC-MGLLS achieved estimates of V_d with low sensitivity to noise levels. Overestimation of V_d was observed to exceed almost 400% for FCM-GLLS and 700% for AFC-GLLS. It was not surprising to observe low reliability of V_d achieved by AFC-GLLS due to the small structure of thalamus giving rise to physiologically meaningless fits with the introduction of inappropriate cluster centroid curves for the generation of the parametric image.

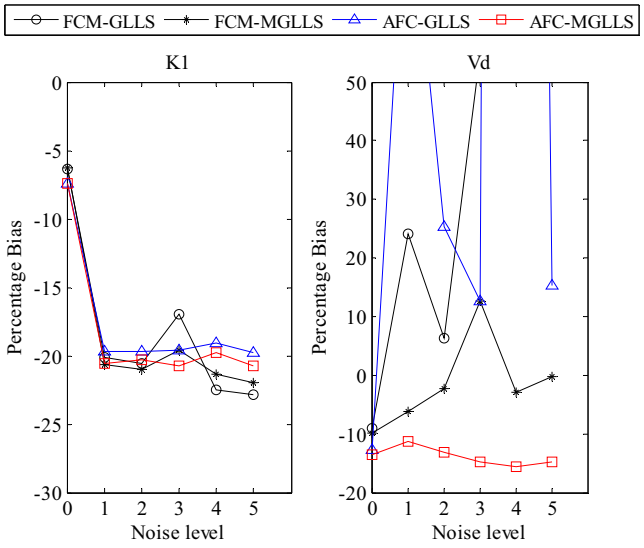

Fig.4. Plots of percentage bias for the thalamus as a function of increasing noise level without the normalization of TTAC. Same legend descriptions as Fig.3.

The above results demonstrated that AFC improved estimated reliability of parametric images using GLLS because the introduced gradual level in AFC improved SNR with less number of clusters. However, low SNR in noisy functional imaging still led to unreliable parametric image of V_d for GLLS fitting with AFC. For MGLLS with enhanced reliability performance, AFC demonstrated slightly increased bias compared with standard FCM. Interestingly, AFC-MGLLS was observed to achieve the most consistent parameter estimate of V_d for a small structure (the thalamus).

B. *Effect of the Normalization*

When the normalization of TTAC was applied with clustering analysis, similar results were observed for the percentage bias and CV for the cerebellum and frontal cortex. However, there was a significant difference for the results of the thalamus shown in Fig.5.

Unexpectedly, K_1 was substantially overestimated by AFC for both GLLS and MGLLS in contrast to the estimates for the noise free data. This implied the integration of the normalization of TTAC and AFC would sacrifice estimated accuracy of K_1 for small structures to achieve physiologically meaningful fits.

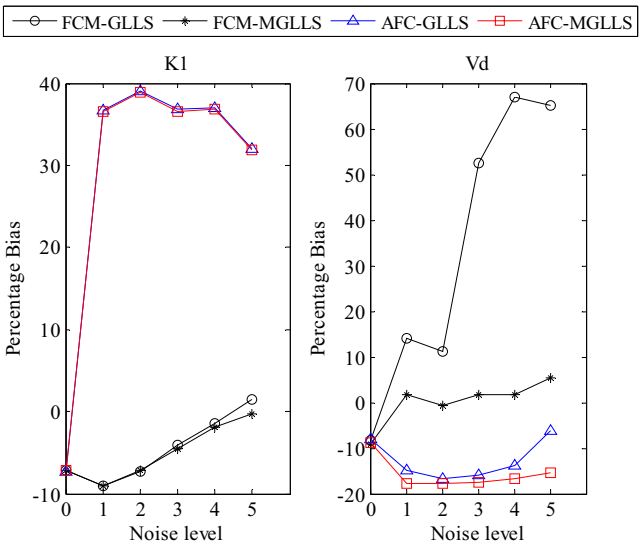

Fig.5. Plots of percentage bias for the thalamus as a function of increasing noise level with the normalization of TTAC. Same legend descriptions as Fig.3.

C. *Computational Cost*

The analysis was performed using an in-house program written in IDL (RSI Inc, Boulder, CO, USA) on a Sun Fire X4200 server (CPU: 2.6GHz, Memory: 16 GB). Table I lists the averaged computational cost for processing one data set.

TABLE I
COMPUTATIONAL COST OF CLUSERING ANALYSIS WITH GLLS AND MGLLS

(min)	FCM-GLLS	FCM-MGLLS	AFC-GLLS	AFC-MGLLS
Non #	417.6	419.8	13.2	15.4
Norm ^	102.0	106.4	3.1	5.4

Non: without normalization. ^ Norm: with normalization.

The use of the normalization of TTAC led to about four-fold reduction in computational cost both for FCM and AFC. In contrast, AFC achieved a marked 30-fold reduction of computational cost compared with standard FCM for the data without normalization.

IV. CONCLUSION

Our proposed adaptive fuzzy clustering introduces levels in standard fuzzy clustering with less numbers of clusters. The quantitative analysis of the simulation results show that AFC provides improved reliable parametric images for low-SNR functional imaging compared with the standard FCM method with about 30-fold improvement in computational efficiency, but at the expense of slight underestimation of K_1 at higher noise levels. AFC with MGLLS showed more consistent parameter estimate of V_d for small structures, like the thalamus. Despite of the improved computational efficiency achieved, the normalization of TTAC may lead to severe overestimation for small structures when AFC is applied. Overall, the enhanced MGLLS method with AFC shows the best performance for generating reliable parametric images. Further investigation to determine the optimal number of

levels and clinical performance are warranted to maximize benefits from functional imaging.

ACKNOWLEDGMENT

This work was partially supported by the ARC, PolyU/UGC, NSFC grants, and the Australia-China special fund of the Australian international science linkage.

REFERENCES

[1] D. Feng, *Biomedical Information Technology*, San Diego: Elsevier press, 2007.

[2] L. Wen, S. Eberl, K. P. Wong, et al., "Effect of reconstruction and filtering on kinetic parameter estimation bias and reliability for dynamic SPECT: A simulation study," IEEE Transactions on Nuclear Science, vol. 52, pp. 69-78, 2005.

[3] X. Li, D. Feng, and K. Chen, "Optimal image sampling schedule: A new effective way to reduce dynamic image storage space and functional image processing time," *IEEE Transactions on Medical Imaging*, vol. 15, pp. 710-719, 1996.

[4] A. K. Jain, M. N. Murty, and P. J. Flynn, "Data clustering: A review," *Acm Computing Surveys*, vol. 31, pp. 264-323, 1999.

[5] R. Xu and D. Wunsch, "Survey of clustering algorithms," *IEEE Transactions on Neural Networks*, vol. 16, pp. 645-678, 2005.

[6] D. L. Pham and J. L. Prince, "Adaptive fuzzy segmentation of magnetic resonance images," *IEEE Transactions on Medical Imaging*, vol. 18, pp. 737-752, 1999.

[7] K. P. Wong, D. G. Feng, S. R. Meikle, et al., "Segmentation of dynamic PET images using cluster analysis," *IEEE Transactions on Nuclear Science*, vol. 49, pp. 200-207, 2002.

[8] H. Zaidi, M. Diaz-Gomez, A. Boudraa, et al., "Fuzzy clustering-based segmented attenuation correction in whole-body PET imaging," *Physics in Medicine and Biology*, vol. 47, pp. 1143-1160, 2002.

[9] Y. Kimura, H. Hsu, H. Toyama, et al., "Improved signal-to-noise ratio in parametric images by cluster analysis," *Neuroimage*, vol. 9, pp. 554-561, 1999.

[10] Y. Kimura, M. Senda, and N. M. Alpert, "Fast formation of statistically reliable FDG parametric images based on clustering and principal components," *Physics in Medicine and Biology*, vol. 47, pp. 455-468, 2002.

[11] H. Bal, E. V. R. Dibella, and G. T. Gullberg, "Parametric image formation using clustering for dynamic cardiac SPECT," *IEEE Transactions on Nuclear Science*, vol. 50, pp. 1584-1589, 2003.

[12] L. Wen, S. Eberl, D. Feng, et al., "Fast and Reliable Estimation of Multiple Parametric Images Using an Integrated Method for Dynamic SPECT," *IEEE Transactions on Medical Imaging*, vol. 26, pp. 179-189, 2007.

[13] L Wen, S Eberl, D Feng. "Reliable model and cluster aided formation of parametric images in functional imaging", *Proceeding of the 17th IFAC World Congress*, pp.6669-6674. Seoul, Korea, 6-11 July, 2008.

[14] L. Wen, S. Eberl, and D. Feng, "Fast and reliable parametric image formation using adaptive fuzzy clustering," presented at SNM Annual Meeting, New Orleans, USA, 2008.

[15] D. Feng, S.-C. Huang, Z. Wang, et al., "An Unbiased Parametric Imaging Algorithm for Nonuniformly Sampled Biomedical System Parameter Estimation," *IEEE Transactions on Medical Imaging*, vol. 15, pp. 512-518, 1996.

[16] L. Wen, S. Eberl, and D. Feng, "A flexible model aided GLLS method for enhanced parameter estimation reliability in SPECT," presented at SNM Annual Meeting, Washington DC, USA, 2007.

[17] M. Kassiou, S. Eberl, S. R. Meikle, et al., "In vivo imaging of nicotinic receptor upregulation following chronic (-)-nicotine treatment in baboon using SPECT," *Nuclear Medicine and Biology*, vol. 28, pp. 165-175, 2001.

[18] I. G. Zubal, C. R. Harrell, E. O. Smith, et al., "Computerized 3-dimensional segmented human anatomy," vol. 21, pp. 299-302, 1994.

[19] H. M. Hudson and R. S. Larkin, "Accelerated image reconstruction using ordered subsets of projection data," vol. 13, pp. 601-609, 1994.